ELSEVIER

Contents lists available at ScienceDirect

NeuroImage

journal homepage: www.elsevier.com/locate/ynimg





Putamen vascularization on high-resolution 7T MRI is associated with perfusion and cognitive performance in cerebral small vessel disease

Philipp Arndt a,b,1,* , Stefanie Boewe a,1, Jascha Brüggemann , Berta Garcia-Garcia b, Renat Yakupov a,b, Niklas Vockert b, Anne Maas b, Malte Pfister a, Valentina Perosa b,d, Marwa Al Dubai a, Robin Jansen e, Sven G. Meuth e, Marc Dörner b,f, Patrick Müller g, Solveig Henneicke a,b, Frank Schreiber a,b, Katja Neumann a, Hendrik Mattern b,c,h,1, Stefanie Schreiber a,b,h,1

- ^a Department of Neurology, Otto-von-Guericke University, Magdeburg Germany
- ^b German Center for Neurodegenerative Diseases (DZNE), Magdeburg, Germany
- ^c Biomedical Magnetic Resonance, Otto von Guericke Universität, Magdeburg, Germany
- ^d J. Philip Kistler Stroke Research Center, Massachusetts General Hospital/Harvard Medical School, Boston, USA
- ^e Department of Neurology, Heinrich-Heine-University, Düsseldorf, Germany
- f Department of Consultation-Liaison-Psychiatry and Psychosomatic Medicine, University Hospital Zurich, University of Zurich, Zurich, Switzerland
- ^g Department of Cardiology, Otto-von-Guericke University, Magdeburg Germany
- ^h Center for Behavioral Brain Sciences, Magdeburg, Germany

ARTICLE INFO

Keywords: Cerebral small vessel disease Vessel distance mapping Cognition Lenticulostriate arteries Putamen Basal ganglia Arterial spin labelling

ABSTRACT

Objective: In cerebral small vessel disease (CSVD), compromised arterial supply to the deep gray matter contributes to cognitive decline. While CSVD frequently involves lenticulostriate arteries supplying the putamen, the functional consequences of altered putaminal vascular architecture remain unclear. We hypothesized that a less homogeneous arterial network in the putamen is associated with impaired perfusion and worse cognitive performance in CSVD.

Methods: We enrolled 16 CSVD patients with cerebral microbleeds and 21 age-matched controls (mean age 71 years; 38 % female). High-resolution 7 T time-of-flight angiography was used to segment all visible intraputaminal vessels. For each voxel in the putamen, the distance to its nearest segmented vessel was computed to generate a vessel distance map; the mean vessel distance reflects the homogeneity of the arterial network. Putaminal perfusion was quantified via multi-inversion time pulsed arterial spin labeling (ASL) at 3 T, and CSVD severity was scored on clinical 3 T MRI. All participants completed a comprehensive neuropsychological battery to derive a global cognition composite score.

Results: Linear regression revealed that higher CSVD MRI scores predicted larger mean vessel distance, reflecting a sparser arterial network, in both the right (B = 0.12, β = 0.42, p = 0.010) and left putamen (B = 0.13, β = 0.43, p = 0.014). Across all participants, increased vessel distance was also associated with prolonged arterial transit time in the right (B = 0.044, β = 0.50, p = 0.009) and left putamen (B = 0.042, β = 0.49, p = 0.009). Finally, in a multivariable linear regression adjusting for demographics, vascular risk factors, and CSVD severity, greater vessel distance in the right putamen was associated with lower global cognitive performance (B = -1.26, β = -0.34, p = 0.012).

Conclusion: This study demonstrates the impact of an impaired arterial network in the putamen on blood supply and cognitive function across the continuum of CSVD.

Abbreviations: RAH, recurrent artery of Heubner; LSA, lenticulostriate artery; MMSE, Mini Mental status examination; MoCA, Montreal Cognitive Assessment; ADAScog, Alzheimer's Disease Assessment Scale cognitive subscale; CSVD, cerebral small vessel disease; ToF, time-of-flight; VDM, vessel distance mapping; CMB, cerebral microbleeds; MRI, magnetic resonance imaging; ICH, intracerebral haemorrhage; WMH, white matter hyperintensities; PVS, perivascular spaces; BG, basal ganglia; MPRAGE, magnetization-prepared rapid gradient echo; SD, standard deviation; IQR, interquartile range.

E-mail address: ph.ulbrich@web.de (P. Arndt).

Corresponding author.

¹ equally contributed first/last authorship.

P. Arndt et al. NeuroImage 319 (2025) 121426

1. Introduction

Cerebral small vessel disease (CSVD) affects the microvasculature of the brain and is characterized by haemorrhagic and non-haemorrhagic lesions on magnetic resonance imaging (MRI) (Duering et al., 2023). Ischemic and haemorrhagic stroke and cognitive impairment are major consequences of CSVD (Li et al., 2018). Of these sequelae, cognitive impairment represents an important clinical outcome, with impact on quality of life and a significant socio-economic burden (Fernando et al., 2021; Meng et al., 2019; Østergaard et al., 2016). Despite its clinical relevance, the precise pathomechanisms leading to cognitive impairment in CSVD remain incompletely understood.

Recent advances in high-resolution neuroimaging have provided novel insights into the role of neurofluid circulation and vascular integrity in maintaining cognitive function. The morphology of small arteries in deep brain regions, such as the hippocampus, is emerging as a critical contributing factor to cognitive resilience, especially in individuals with CSVD (Perosa et al., 2020; Vockert et al., 2021). Similarly, morphological changes in the lenticulostriate arteries (LSA), which supply the basal ganglia, have been observed in CSVD and are thought to contribute to the disease's pathophysiology (Chen et al., 2019). These perforating arterioles are particularly susceptible to arteriolosclerosis and lack effective collaterals, making deep brain regions vulnerable to downstream consequences of microvascular pathology, including lacunar infarcts, cerebral microbleeds (CMB), and enlarged perivascular spaces (PVS), ultimately leading to tissue damage (Cho et al., 2008; Marinkovic et al., 2001; Mehrnoosh Ghandili and Sunil Munakomi, 2022; Perosa et al., 2020).

Microvascular pathologies on MRI are typically found in the putamen and have been linked to cognitive impairment in CSVD (Huijts et al., 2014; Li et al., 2021; Patel and Markus, 2011). While the putamen is classically associated with motor execution and motor learning, accumulating evidence highlights its role as a key hub in neuronal processing, contributing to higher-order cognitive functions such as global cognition, memory, attention, executive function, and reward processing (Afifi, 2003; Ell et al., 2011; Max et al., 2002; Schultz, 2016; Tortorella et al., 2013; Viñas-Guasch and Wu, 2017). Functional MRI studies have demonstrated that neural activity in the putamen is reduced in CSVD and correlates with cognitive impairment (Feng et al., 2021; Zhang et al., 2023). However, whether reduced arterial vascularization of the putamen underlies cognitive dysfunction via impaired neurofluid circulation remains unclear.

To address this gap, we investigated the relationship between intraputamen arterial vascularization, perfusion dynamics, and cognitive performance in patients with CSVD and cognitively unimpaired controls. This study aligns with the scope of the special issue on "Emerging Methods for Mapping Neurofluid Circulation and Exchange", as it applies advanced high-resolution 7T MRI techniques to assess microvascular structure, function and its impact on cognition. Specifically, we leveraged 7T time-of-flight (ToF) MR angiography to visualize intraputamen arteries and employed vessel distance mapping (VDM) - an innovative image post-processing technique that quantifies the shortest distance of each voxel to its nearest artery (Garcia-Garcia et al., 2023). This approach enables a novel, tissue-centered perspective of vascularization, shifting focus from vessel morphology alone to the spatial distribution of arteries relative to brain tissue, which is critical for effective fluid circulation and tissue supply.

2. Material and methods

2.1. Study design and participants

A total of 51 older adults were included in this prospective 7T brain MRI study. The scans were acquired between December 2016 and July 2018. Details on inclusion and exclusion criteria have been explained recently (Perosa et al., 2020). In short, patients were recruited from a

longitudinal 3T MRI study on the pathophysiology of CSVD conducted at the University Clinic of Magdeburg and the German Center for Neurodegenerative Disease (DZNE), Magdeburg. Inclusion criteria for CSVD patients were the presence of haemorrhagic CSVD markers, including CMB or intracerebral haemorrhage (ICH) on iron-sensitive MRI sequences (GRE T2*-weighted or susceptibility-weighted imaging). Controls were considered as such if they had no haemorrhagic markers on 3T MRI and were recruited from an already existing pool of cognitively normal community-dwelling elderly study participants of the DZNE Magdeburg. Out of 51 participants, 37 (16 CSVD patients, 21 controls) were included for the final analysis (Fig. 1). Three were excluded due to missing data for neuropsychological tests, four due to MRI sequences for arterial segmentation with motion artifacts and in seven no suitable arterial segmentation could be created, since the sequence originally covered only a certain part of the brain (for details see below). All participants provided written informed consent according to the Declaration of Helsinki and were compensated for travel costs. The study was approved by the local Ethics Committee (93/17; 28/16).

2.2. Clinical data

Participants were characterized with regard to a history of symptomatic ischemic stroke or symptomatic intracerebral haemorrhage. Data on age, sex, years of education were available for all participants; data of vascular risk factors were missing for two participants. Vascular risk factors were defined by prior diagnosis of arterial hypertension, dyslipidemia and type 2 diabetes or antihypertensive, lipid lowering or antidiabetic medication. Additionally, we considered clinical laboratory blood tests for dyslipidemia (total cholesterol $>5.2\ mmol/L$, LDL cholesterol $>2.6\ mmol/L$, HDL cholesterol $<1.0\ mmol/L$ or triglycerides $>1.7\ mmol/L$) and type 2 diabetes (HbA1c $\geq6.5\ \%$ or fasting plasma glucose level $\geq7.0\ mmol/L$).

2.3. Neuropsychological testing

All participants underwent a neuropsychological test battery comprising Clinical Dementia Rating (CDR) (Morris, 1993), Mini-Mental State Examination (MMSE) (Folstein et al., 1975), Montreal Cognitive Assessment (MoCA) (Nasreddine et al., 2005) and Alzheimer's Disease Assessment Scale-Cognitive Subscale (ADAS-Cog) (Rosen et al., 1984). According to MMSE and CDR, all controls and 7 CSVD patients were

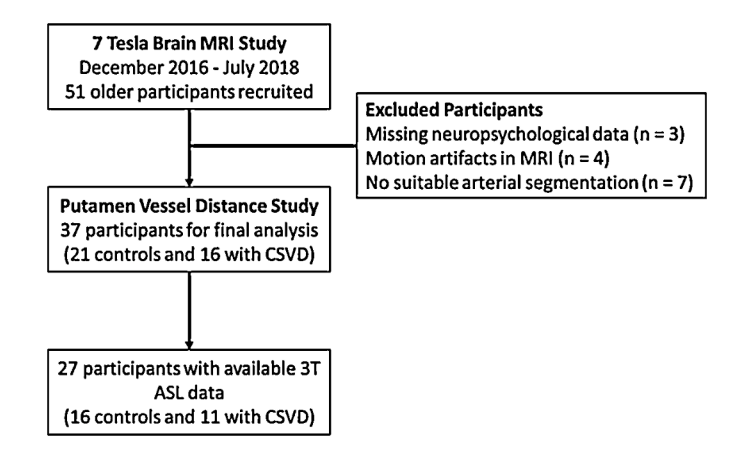


Fig. 1. Flowchart of participant inclusion and exclusion for the study cohort. A total of 51 older adults were initially recruited for this study. Of these, 3 participants were excluded due to missing neuropsychological data, 4 were excluded due to motion artifacts in MRI sequences, and 7 were excluded because no suitable arterial segmentation could be created. The final analysis included 40 participants (16 CSVD patients and 21 controls). In a subset of 27 participants 3T ASL data were available to assess perfusion in the putamen. Detailed inclusion and exclusion criteria are described in the methods section.

cognitively unimpaired (MMSE > 26, CDR = 0), 8 CSVD patients fulfilled the criteria for mild cognitive impairment (MMSE 21 to 26, CDR 0.5 to 1) and one patient had mild dementia (MMSE = 19; CDR = 0.5). Neuropsychological testing and MRI were performed a median of 63 days apart (IQR 31–152 days).

In order to obtain a robust measure of global cognitive function, we constructed a composite score using z-scores for MMSE, MoCA, and ADAS-Cog. For each participant, z-scores were calculated (individual test score minus the mean test score of the control group, divided by the control group's standard deviation). ADAS-Cog z-scores were multiplied by –1 to align the direction of scoring with MMSE and MoCA, where higher values indicate better performance. The composite score was then derived by averaging the three z-scores of each test for each individual (Prins et al., 2005).

2.4. MRI

To diagnose or exclude CSVD, all participants underwent a 3T scan prior to 7T MRI (mean interval 62 days). Measurements were performed in a Siemens Verio scanner. The protocol included a structural wholebrain T1-weighted magnetization prepared rapid acquisition gradient echo (MPRAGE) sequence, a whole-brain 3D fluid attenuated inversion recovery sequence to localize lacunes and evaluate white matter hyperintensities (WMH) (Fazekas et al., 1987) with 1 mm³ isotropic resolution, a susceptibility-weighted 3D gradient-echo pulse sequence to count CMB (voxel size $1 \times 1 \times 2$ mm³) and a high-resolution T2-weighted turbo spin echo sequence with 0.5 mm x 0.5 mm in-plane resolution and slices of 2 mm thickness to rate PVS (Potter et al., 2015).

CSVD was evaluated according to standards for reporting vascular changes on neuroimaging (STRIVE) criteria and whole brain CSVD severity was assessed based on an established scale from 0 to 6, with one point being allocated for the presence of (i) lacunes, (ii) 1 to 4 CMB, (iii) moderate to severe basal ganglia PVS (>10), and (iv) moderate WMH (sum of deep and periventricular WMH grade 3 to 4). Two points were allocated for the presence of (i) \geq 5 CMB or (ii) severe WMH (sum of deep and periventricular WMH grade 5 to 6) (Pasi et al., 2021).

2.5. 7T MRI

All participants underwent a 7T ultrahigh-field MRI scan using a Siemens MAGNETOM 7T scanner equipped with a Nova Medical 32-channel head-coil. The protocol included a T1-weighted 3D MPRAGE (1 mm 3 isotropic resolution, TE 2.89 ms, TR 2250 ms, inversion time 1050 ms, band width 130 Hz/pixel, echo spacing 8.3 ms, 3D matrix dimensions 256 \times 256 \times 176) and a ToF angiography (0.28 mm 3 isotropic resolution, 5 imaging slabs each with 48 slices, TR 22 ms, TE 4.59 ms, band width 142 Hz/pixel, sparse venous saturation (Mattern et al., 2018)). The ToF covered a certain part of the brain only: the origin of the slab was set at the bottom of the hippocampus and extended 5 cm in the dorsal direction, allowing depiction of the circle of Willis and the entire putamen in 47 of 51 participants. Thin pillows were placed at the sides of the participant's head to minimize head motion.

2.6. 7T MRI image processing and analysis

7T T1-weighted MPRAGE and ToF images were converted from DICOM to NIFTI format using the dcm2nii routine of the MRIcron software package (https://www.nitrc.org/projects/mricron). Subsequently, inhomogeneities in the MPRAGE images were corrected using SPM12 (Statistical Parametric Mapping Software, Wellcome Trust Centre for Neuroimaging, London, UK) and MATLAB R2014b (Mathworks, Sherborn, MA, USA). To determine the location of blood vessels in relation to the putamen, an anatomical reference was required. For this purpose, a putamen mask was created for each subject. The structural images were segmented automatically using the subcortical

segmentation pipeline (Fischl et al., 2004) of FreeSurfer 6.0 (https://surfer.nmr.mgh.harvard.edu). A visual inspection of the results was conducted to ensure accurate segmentation of the putamen. The putamen region (left and right) was extracted as a mask and registered to the corresponding ToF images using Advanced Normalization Tools (Avants et al., 2011).

2.7. Arterial segmentation

The vasculature in the putamen was investigated using Mango software, allowing a detailed examination of ToF images in sagittal, coronal, and axial planes. The axial view was used for vessel tracking. The LSA originates from the middle cerebral artery (Seo et al., 2012) and the RAH originates from different segments of the anterior cerebral artery (El Falougy et al., 2013). We assessed for each participant whether the RAH contributed to putamen vascularization in one or both hemispheres.

A comprehensive approach was then employed for manual vessel delineation, using both forward and backward methods to verify truthful segmentation performance (performed by S.B. and B.G.G. with 4 years of experience). This involved locating the origin of each vessel, tracking its branches layer by layer, and confirming complete segmentation through reverse tracking. Complex cases were discussed until reaching a consensus. The precision of this delineation was crucial for subsequent VDM calculations, because VDM is computing distances with respect to the segmented vasculature. Fig. 2 shows the segmented, color-coded vasculature and its trajectory within the putamen. A meticulous retrospective review ensured that no arteries within or in proximity to the putamen were left unsegmented, considering the spatial resolution of the 7T ToF imaging. This methodology aimed to provide a thorough understanding of the vascular architecture within the putamen.

2.8. Vessel density and vessel distance mapping

Vessel density was computed as the relative volume occupied by arterial voxels with respect to the putamen volume. VDM calculates the Euclidean distance of each voxel to its nearest blood vessel by applying distance transformation to the vessel segmentation. The distance measure determines, for each voxel, how close the nearest blood vessel is in millimetres. Similar to vessel densities, VDM captures the abundance of detected/segmented vessels while simultaneously considering the spatial patterns of blood vessels as well (Garcia-Garcia et al., 2023). One has to keep in mind that all identified vessels were included, regardless of their specific origin, such as LSA or recurrent artery of heubner (RHA). Resilient tissue voxels should have low VDM values, indicating that they are close to a vessel

(Garcia-Garcia et al., 2023). All VDM metrics are pure distance metrics and are based on the processing of structural data. VDM was averaged per putamen. Hence, VDM is based on the premise that spatial proximity correlates with the probability of vascular supply (Feekes et al., 2005; Garcia-Garcia et al., 2023).

2.9. Cerebral blood flow and arterial transit time

For a subgroup of 27 participants, a multi-inversion time pulsed arterial spin labelling (ASL) sequence was available with FAIR labelling, 3D-GRASE readout and Q2TIPS background suppression. The pulsed ASL protocol included the following parameters: 4 mm x 4 mm in-plane resolution, TR/TE = 3600/22.82 ms, 16 slices of 5.5 mm thickness, bolus length = 1400 ms, 13 TIs ranging from 300 ms to 2700 ms with an increment of 200 ms and five proton density weighted M0 calibration scans with TR = 4360 ms. ASL MRI data analyzed using the FSL's BASIL tool (Chappell et al., 2010, 2009; Groves et al., 2009) employing the general kinetic model (Buxton et al., 1998). This step included a registration of all tag-control image pairs and reference scans (Jenkinson et al., 2002), a partial volume correction (Chappell et al., 2011) which incorporates the different temporal characteristics of the ASL signal for

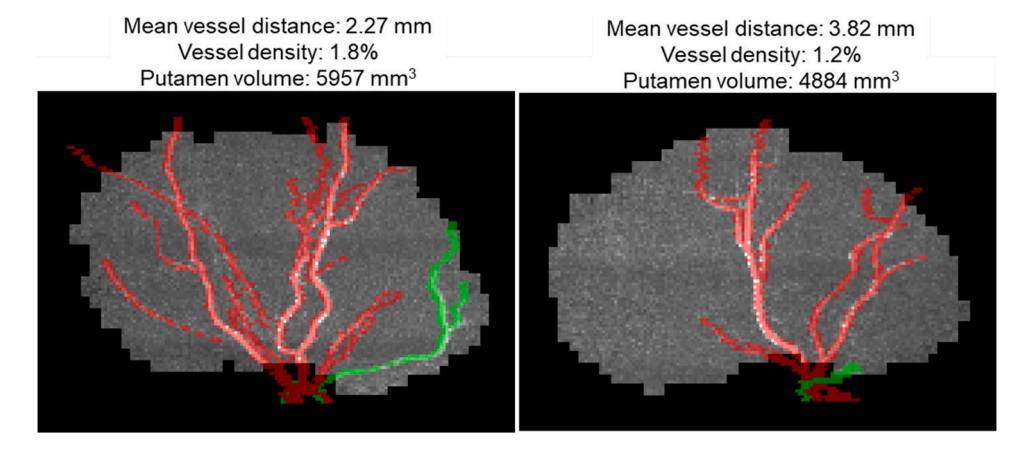


Fig. 2. Arterial Segmentation within the putamen. Two exemplary images presenting participants with high (left) and low (right) vessel density. The images represent two-dimensional maximum intensity projections of time-of-flight angiography signal in the putamen with a color-coded overlay of vessel segmentation (lenticulostriate arteries in red, recurrent artery of Heubner in green). The numerical values for mean vessel distance, vessel density, and putamen volume are shown as well

different tissue-types obtained from structural T1 weighted images, and a calibration with M0 scans to quantify CBF in mL/100 g/min and ATT in $^{\rm s}$

To calculate mean perfusion (CBF, ATT) values for the putamen, 7T TOF sequences were co-registered to the respective 3T MPRAGE space using the co-registration algorithms provided in SPM 12, applying the normalized mutual information cost function and nearest neighbor interpolation. The resulting transformation was consequently applied to the binarized Putamen mask used in the 7T TOF analysis. These masks were then applied to the prior estimated perfusion maps. For illustration, a representative example of the CBF and ATT maps is provided in **Supplementary Figure 1**.

2.10. Statistical analysis

Results of continuous or ordinal variables were expressed as mean (standard deviation, SD) or median (IQR); results of categorical variables were expressed as proportions. Intergroup comparisons between CSVD patients and controls were performed in univariate analyses, using the χ^2 -test, Man-Whitney U test or 2-sample t-test, as appropriate. For all analyses, right and left putamen were considered separately. Right and left hemispheric putamen vessel distance was compared with a paired t-test to test for differences within participants.

To investigate whether the CSVD severity (MRI score, independent variable) was independently associated with vessel distance in the left and right putamen (dependent variable), multivariate linear regression analyses were performed and adjusted for age, sex, years of education, and number of vascular risk factors.

We next investigated the relationship between putamen vascularization and perfusion applying linear regression analysis in a subset of 27 participants (16 controls, 11 CSVD patients) with available data.

Finally, we hypothesised an independent effect of putamen vascularization on cognition. Therefore, we tested whether putamen vascularization (independent variable) was related to the global cognition composite score (dependent variable) in multivariate linear regression models, adjusted for age, sex, years of education, vascular risk factors, and CSVD MRI score. The analyses were repeated within subgroups to identify drivers of the association.

Within each hypothesis set p-values were additionally adjusted for multiple testing using the Benjamini–Hochberg false discovery rate (BH-FDR) procedure. The corresponding q-values were calculated based on (i) 2 tests for CSVD severity \rightarrow vessel distance, (ii) 4 tests for vessel distance \rightarrow perfusion, and (iii) 2 tests for vessel distance \rightarrow cognition, and are reported in **Supplementary Table 1**.

Collinearity statistics were applied to identify issues of multicollinearity. These showed no evidence of multicollinearity in all regression models. For all regression models, we reported unstandardized (B) and standardized (β) regression coefficients. Significance level was set at 0.05 for all analyses. IBM SPSS Statistics 24.0 software was used for all analyses.

3. Results

We included 16 patients with symptomatic CSVD (2 with strictly deep hemorrhages, 7 with mixed location hemorrhages and 7 with strictly lobar hemorrhages) and 21 age-matched, cognitively unimpaired control participants without hemorrhages. Clinical diagnoses of CSVD patients comprised cognitive impairment (n = 9, 56 %), symptomatic ischemic stroke (n = 6, 38 %) and symptomatic ICH (n = 6, 33%). Participants had a mean age of 71.0 years and 14 (38 %) were female. Compared to controls, patients with CSVD had more vascular risk factors (median 2 vs. 1, p = .025), driven by hypertension (88 % vs. 57 %, p = .017), and a higher CSVD MRI score (median 4 vs. 0, p < .001), driven by higher numbers of CMB (median 0 vs. 8, p < .001), advanced WMH (median Fazekas score 4 vs. 2, p < .001) and lacunes (present in 63 % vs. 5 %, p < .001). CSVD patients performed worse in neuropsychological tests for global cognitive function when compared to controls (mean global cognition composite score: -2.96 vs. 0.00, p < .001). Key characteristics and statistical group comparisons between controls and CSVD patients are shown in Table 1.

By using high-resolution ToF angiography at 7T MRI, we assessed the arterial vascularization of the putamen qualitatively and quantitatively. Qualitatively, the putamen is supplied by LSA and in some individuals additionally by the RAH, contributing to the supply of both hemispheres in 10 (27 %) participants, of one hemisphere in 17 (46 %) participants and was absent in 10 (27 %) participants. The prevalence of none, one or two RHA contributing to putamen vascularization did not differ between controls and CSVD patients. Subsequently, the supplying arteries were segmented to quantitatively assess the arterial vessel density (proportion of volume) and spatial distribution (average distance of each voxel to its nearest artery) within the putamen. Both vascular metrics were highly related to each other across all participants (right putamen: β -0.73, p < .001; left putamen: $\beta = -0.79$, p < .001), and within subgroups (controls: right putamen $\beta = -0.51$, p = .015 and left putamen β = -0.76, p < .001; CSVD: right putamen $\beta = -0.81$, p < .001 and left putamen: $\beta = -0.83$, p < .001). Vessel segmentations for each participant with the corresponding mean vessel distance, vessel density and putamen volume values are shown in Supplementary Figure 2 and 3.

Table 1 Group comparison of key patient characteristics. Data are presented as mean (SD), median (IQR) or proportions. Significant p-values are marked in bold. IQR, interquartile range; SD, standard deviation; VDM, vessel distance mapping. ^a Data are available for 27 participants only (16 controls, 11 CSVD patients).

		, (10 00111 010, 11			
	Controls	CSVD	test	P-value	
	n=21	n = 16	statistic		
Demographics					
Age	70.5 (7.6)	71.8 (6.4)	T = -0.53	.603	
Female sex	10 (48 %)	4 (25 %)	$X^2 = 1.98$.160	
Years of education Vascular risk factors	16.1 (2.6)	14.5 (4.1)	T = 1.44	.164	
Number of vascular risk factors	1 (1–2)	2 (1–3)	Z = 2.34	.025	
Hypertension	12 (57 %)	14 (88 %)	$X^2 = 5.71$.017	
Dyslipidaemia	8 (38 %)	9 (56 %)	$X^2 = 1.69$.194	
Type 2 diabetes	3 (14 %)	4 (25 %)	$X^2 = 0.86$.355	
MRI CSVD markers			0.00		
CSVD MRI score	0 (0-1)	4 (3–5)	Z = 5.03	< 0.001	
Total number of CMB	0 (0–0)	8 (2–17)	Z = 5.43	< 0.001	
WMH Fazeka grade [0–6]	2 (1–3)	4 (3–6)	Z = 3.83	< 0.001	
Presence of lacunes	1 (5 %)	10 (63 %)	$X^2 = 14.49$	<0.001	
Deep lacunes	0 (0 %)	8 (50 %)	$X^2 = 13.40$	<0.001	
Lobar lacunes	1 (5 %)	9 (56 %)	$X^2 = 12.21$	<0.001	
BG PVS grade [0-4]	1 (1-1)	2 (1-4)	Z = 1.86	.089	
CSO PVS grade [0–4]	2 (2–3)	2 (1-4)	Z = 1.00	.728	
GBO I VB Grade [0 1]	2 (2 3)	2(1 1)	-0.367	.720	
Neuropsychological a	ssessment		0.007		
Global cognition composite score	0.00 (0.67)	-2.96 (2.25)	T = 5.16	<0.001	
MMSE	28.8 (1.2)	25.3 (2.7)	T = 4.95	< 0.001	
MoCA	27.4 (2.5)	21.8 (4.0)	T = 5.00	< 0.001	
ADAScog	6.5 (2.1)	14.3 (6.8)	T =	< 0.001	
-4.44					
Putamen vascularizati Volume right	5845	6100	Z = 1.56	.123	
putamen [mm ³]	(5356–6360)	6188 (5677–6881)	Z = 1.30	.123	
Volume left putamen	5838	5842	Z = 1.04	.308	
[mm ³]	(5265-6180)	(5275-6697)			
Vessel density right putamen [%]	1.6 (0.2)	1.6 (0.5)	T = 0.34	.738	
Vessel density left putamen [%]	1.8 (0.5)	1.7 (0.5)	T = 0.65	.518	
Vessel distance right putamen [mm]	3.1 (0.4)	3.4 (0.8)	T = -1.58	.130	
Vessel distance left putamen [mm]	2.9 (0.4)	3.2 (0.8)	T = -1.48	.155	
Putamen [mm] —1.48 Putamen perfusion on 3T MRI ^a					
CBF right putamen [mL/100 g*min]	73.5 (16.7)	65.9 (16.8)	T = 1.15	.260	
CBF left putamen [mL/100 g*min]	74.3 (15.9)	69.1 (18.8)	T = 0.77	.445	
ATT right putamen [s]	0.42 (0.04)	0.46 (0.06)	T = -2.13	.043	
ATT left putamen [s]	0.44 (0.05)	0.45 (0.06)	T = -0.59	.564	

Putamen volume, vessel density and mean distance to arteries did not differ between the groups, but in a subgroup of 27 participants with available 3T ASL data (16 controls and 11 patients with CSVD) ATT in the right putamen was significantly increased in CSVD patients compared to controls (mean 0.46 vs 0.42, p=.043). There were no significant differences in CBF and ATT in the left putamen (Table 1). Within participants, there were no significant differences in mean vessel distance between left and right hemisphere (data not shown).

3.1. CSVD severity predicts larger vessel distance in the putamen

To investigate whether CSVD is independently associated with larger vessel distance in the putamen, linear regression analyses were conducted. The CSVD MRI score, a measure of brain-wide CSVD severity, was significantly associated with larger vessel distance in the right and left putamen across all participants. For each one-point increase in the CSVD score, the mean vessel distance increased by 0.12 to 0.13 mm (right putamen: B=0.12, $\beta=0.42$, p=.010; left putamen: B=0.13, $\beta=0.43$, p=.014), independent of demographics and vascular risk factors, which were controlled for as confounding variables between CSVD patients and controls (Table 2). Including putamen volume as a covariable in the model, the association between the CSVD MRI score and larger vessel distance was no longer significant (right putamen: p=.093; left putamen: p=.116) but notably, putamen volume itself was no significant predictor of vessel distance (right putamen: p=.077; left putamen: p=.082) as well.

3.2. Vessel distance is associated with compromised perfusion

3T ASL MRI data were available for a subgroup of 27 participants (16 controls, 11 CSVD patients) and were used to estimate mean CBF and ATT in the putamen. To support our premise that poor vascularization is related to compromised perfusion, we conducted a linear regression analysis of vessel distance and perfusion parameters in the putamen. Vessel distance was positively associated with ATT in the right (B=0.044, $\beta=0.50$, p=.009) and left putamen (B=0.042, $\beta=0.49$, p=.009), but not with CBF (right putamen: B=-10.36, $\beta=-0.38$, p=.053; left putamen: B=-6.12, $\beta=-0.25$, p=.219) (Fig. 3). This indicates that poor vascularization leads to a prolonged delivery time of blood to reach the tissue, but it might not impact the overall quantity of blood.

3.3. Larger vessel distance is associated with poor cognitive function

Increased mean putamen vessel distance seems to be related to altered blood supply and could in that influence neuronal and subsequently cognitive function. Linear regression across all individuals was utilized to determine whether vessel distance in the putamen is also associated with the cognitive composite score. Indeed, larger mean vessel distance in the right putamen was independently associated with lower scores in global cognition (per increase of 1 mm: B=-1.26, $\beta=-0.34$, p=.012), accounting for demographics, vascular risk and CSVD severity (Table 3, Fig. 4). There was no significant association between vessel distance in the left putamen and cognitive performance (p=.680,

Table 2Associations of CSVD severity with vessel distance in the right and left putamen. The linear regression analysis evaluated the association of CSVD severity (MRI sum score) with vessel distance in the right putamen. The model was adjusted for demographics and vascular risk.

Dependent Variable	Independent Variable	B (95 % CI)	β	P- value
Vessel distance	Age	0.03 (0.00, 0.05)	0.32	.024
right putamen	Male sex	0.26 (-0.09, 0.60)	0.22	.142
	Years of education	-0.07 (-0.12 ,	-0.42	.006
		-0.02)		
	Vascular risk	-0.25 (-0.46 ,	-0.38	.021
	factors	-0.04)		
	CSVD MRI score	0.12 (0.03, 0.22)	0.42	.010
Vessel distance	Age	0.03 (0.00, 0.05)	0.29	.050
left putamen	Male sex	0.36 (-0.02, 0.74)	0.29	.063
	Years of education	-0.01 (-0.07 ,	-0.06	.711
		0.05)		
	Vascular risk	-0.35 (-0.59 ,	-0.52	.004
	factors	-0.12)		
	CSVD MRI score	0.13 (0.03, 0.23)	0.43	.014

P. Arndt et al. NeuroImage 319 (2025) 121426

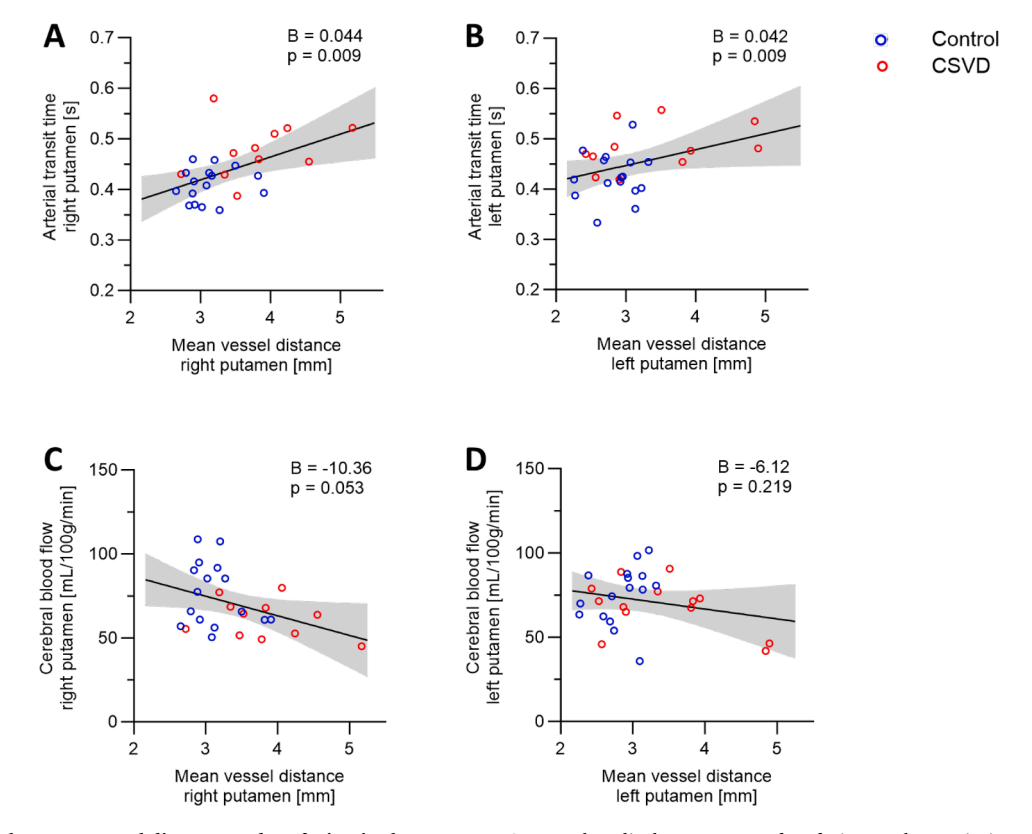


Fig. 3. Associations between vessel distance and perfusion in the putamen. Scatter plots display measures of perfusion on the y-axis, i.e. arterial transit time (A, B) and cerebral blood flow (C, D) and the corresponding vessel distance data on the x-axis. Test statistics are related to a linear regression model. The regression lines are related to all participants, i.e. controls and CSVD patients.

data not shown). This suggests that in terms of poor arterial vascularization participants perform worse in tests for global cognition, even independently of CSVD severity on MRI.

To investigate whether these associations are driven by controls or CSVD patients we repeated the analyses within subgroups. The associations became stronger and remained significant in CSVD patients (B = -1.97, $\beta = -0.66$, p = .013), but not in controls (B = -0.82, $\beta = -0.47$, p = .131).

4. Discussion

This study examined the relationship between CSVD, arterial vascularization of the putamen, and cognitive function. Utilizing high-resolution ToF 7T MR angiography and VDM, we observed that CSVD

Table 3 Associations of vessel distance in the right putamen with cognition. The linear regression analyses evaluated the association of vessel distance in the right putamen with the global cognition composite score. The model was adjusted for demographics, vascular risk and CSVD severity.

Dependent Variable	Independent Variables	B (95 % CI)	β	P- value
Global cognition composite score	Vessel distance right putamen	-1.26 (-2.22, -0.29)	-0.34	.012
-	Age	-0.05 (-0.12, 0.01)	-0.17	.121
	Male sex	-0.38 (-1.31, 0.55)	-0.09	.413
	Years of education	0.01 (-0.14, 0.16)	0.01	.923
	Vascular risk factors	-0.71 (-1.30, 0.11)	-0.29	.022
	CSVD MRI score	-0.46 (-0.73, -0.19)	-0.43	.001

severity is associated with greater average distance to their arteries in the putamen. The increased distance was linked to prolonged ATT and poorer cognitive performance across all participants. These findings suggest that altered vascularization in the putamen contributes to cognitive decline in CSVD.

Our study applied state-of-the-art neuroimaging techniques in combination with neuropsychological testing to study microvascular arterial architecture and neurofluid circulation in the putamen, a brain region highly susceptible to the CSVD, and the consequences for brain function. The combination of ultra-high-field 7T MR angiography with vessel distance allows for a more detailed and quantitative assessment of

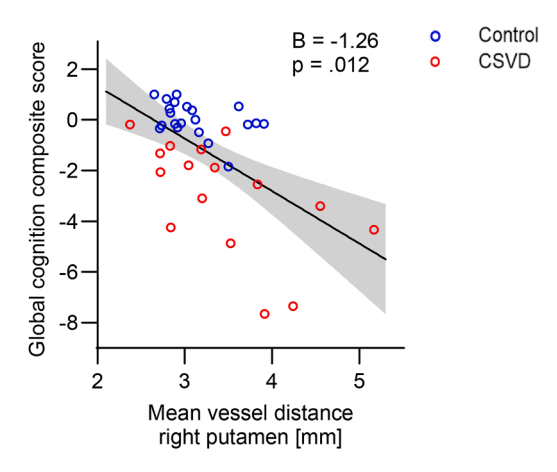


Fig. 4. Associations between vessel distance in the right putamen and the global cognition composite score. Test statistics are related to the fully adjusted linear regression model, accounting for demographics, vascular risk and CSVD severity. The regression line is related to all participants, i.e. controls and CSVD patients.

microvascular architecture beyond conventional approaches that focus solely on large vessel morphology.

Our results demonstrate a significant association between reduced arterial vascularization of the putamen and CSVD severity. These findings align with previous research showing rarefication of LSA branches on invasive digital subtraction angiography or non-invasive MRI in association with CSVD burden (Chen et al., 2019; Jiang et al., 2021; Li et al., 2024). However, it is still uncertain whether poor vascularization of brain tissue is a consequence of microvascular disease, such as due to occlusion of arterial branches, or a congenital factor predisposing individuals to microvascular pathologies. Prospective studies are needed to disentangle this association.

Prior studies assessing the LSA to evaluate deep grey matter vascularization typically focussed on the number of LSA branches and their morphological features (Chen et al., 2019; Jiang et al., 2020; Ling et al., 2019; Wei et al., 2022). While this vessel-centred approach is reasonable, it may overlook the specific requirements of brain tissue. Our study is unique, in that we quantified the spatial distribution of vascularization within a region of interest by measuring the distance of each tissue voxel to its nearest artery. The resulting vessel distance map integrates local vascular supply circumstances and shifts the perspective to a brain tissue-centred view. By shifting the perspective from vessel-centered analyses to a tissue-centered framework, our methodology provides novel insights into how the spatial distribution of microvascular networks influences neurofluid dynamics, and cognition in CSVD.

Recent high-resolution imaging in healthy individuals has demonstrated that structural arterial vascularization and proximity to arteries are directly related to local perfusion at the voxel level in deep grey matter regions, such as the hippocampus (Haast et al., 2024). Building on these insights, increased distance to arteries was associated with prolonged ATT. This association was evident in the left and the right putamen. Interestingly, while ATT was significantly affected, we did not observe a direct relationship between vessel distance and CBF, despite both variables being reliable indicators of brain perfusion (Neumann et al., 2021). This finding suggests that while arterial rarefaction prolongs transit time, it does not necessarily reduce overall blood volume reaching the tissue. However, prolonged ATT could impair metabolic homeostasis during vulnerable periods, such as fluctuations in blood pressure, potentially leading to ischemic injury (Engedal et al., 2018; Takata et al., 2023). Prolonged ATT may also serve as an early marker of impaired perfusion that could precede more significant reductions in CBF, indicating a reliance on less efficient routes or collateral circulation due to narrowing arteries. One large study supports our results and has also shown that reductions in the number of LSA branches are consistently associated with prolonged ATT in the putamen, as measured by computed tomography perfusion (Chen et al., 2019).

The putamen as a part of the basal ganglia has traditionally been linked to motor functions (Graybiel, 2000; Turner and Desmurget, 2010), but accumulating evidence supports its critical role in higher-order cognitive processes (Afifi, 2003; Ell et al., 2011; Max et al., 2002; Schultz, 2016; Tortorella et al., 2013; Viñas-Guasch and Wu, 2017). CSVD can lead to a gradual deterioration of cognitive function (Meng et al., 2019; Østergaard et al., 2016) and typically affects parenchymal small arteries in the putamen (Li et al., 2018; Litak et al., 2020). Additionally, the putamen is highly interconnected and represents a central neuronal hub for information coordination and processing. Tissue damage in CSVD often affects these inter-connected central nodes, leading to a greater disruption of network functionality (Telgte et al., 2018). Changes in structural connectivity of the putamen are driving cognitive impairments and motor deficits in CSVD (Telgte et al., 2018), although the underlying mechanisms remain elusive. To better understand the pathomechanisms contributing to cognitive decline in CSVD, measures of vascularization and CSVD severity were combined with neuropsychological assessments. Our results showed a significant association between compromised arterial vascularization in the right putamen and cognitive performance, independently of confounding

variables such as demographics, vascular risk factors and CSVD severity. Our results suggest that arterial vascularization within the putamen may be closely linked to cognitive function in CSVD. While this association is robust even after adjusting for confounding variables, it is important to consider that vascularization and cognition may not be directly related in a purely causal manner. For instance, shared underlying processes, such as disruption of neuronal networks or neurovascular coupling, could affect both vascular structure and cognitive performance simultaneously. Despite this complexity, our findings support the concept of effective vascularization as a potential brain reserve mechanism. A well-vascularized neural environment may provide better metabolic support and enhance resilience against neurodegenerative and cerebrovascular pathologies (Perosa et al., 2020). Notably, for the left putamen we did not observe this association and one can only speculate that vascular rarefaction might have to reach a certain threshold to compromise tissue supply and thereby neuronal and cognitive functions.

Of note, our study specifically focused on CSVD patients with hemorrhagic markers, representing an advanced and more severe stage of disease. Because of that our findings may not be fully generalizable to all CSVD patients. It is possible that in less advance disease stages, e.g. in individuals with moderate WMH but without hemorrhagic markers, the associations between putamen vascularization and cognition could differ. Future studies in more diverse populations of CSVD patients may investigate whether arterial vascularization differs already in early stages of the disease and whether it may predict cognitive impairment.

4.1. Limitations

Our data are cross-sectional and derived from a small sample. Due to the small sample size, these findings should be interpreted with caution, and replication in larger cohorts is necessary to confirm the robustness of these results and establish their generalizability. Further, prospective studies are needed to understand the causal relationship between vascularization, CSVD progression and cognitive decline. We did not assess whether certain anatomical regions within the putamen are especially affected by increased vessel distance. Further, metrics for vascularization, depend on the depicted and subsequently segmented vasculature. While 7T ToF-MRA at 0.28 mm isotropic primarily resolves small penetrating arteries such as the lenticulostriate arteries (300-700 μm) and offers substantially greater detail than clinical scanners, true arteriolar imaging remains beyond current in-vivo resolution. Despite rigorous segmentation checks, potential biases from imaging artifacts (e. g., motion-induced blurring, partial voluming) represent a potential bias. Moreover, ASL MRI suffers from an intrinsically low signal-to-noise ratio, which might have affected the estimated mean perfusion values (CBF, ATT) of the putamen. However, a reliability analysis in our lab based on an identical ASL sequence and protocol on healthy young participants found a substantial agreement of repeated measures for CBF and ATT (e.g. within-subject coefficient of variation less than 5 % for mean CBF and mean ATT in the hippocampus) (Neumann et al., 2021). We did not include motor assessments and consequently we cannot determine whether the association between putaminal vascularization and global cognition is direct or mediated by motor or fronto-striatal network dysfunction. Finally, the pathophysiology of CSVD is complex and our multimodal approach that integrates disease severity, vascular structure, resting state perfusion and cognitive function, is still limited in making causal conclusions. Important functionally relevant variables such as cerebrovascular reactivity and neuronal network activity based on functional MRI and the importance of other brain regions need to be integrated into the complex construct.

4.2. Outlook

Future studies should focus on longitudinal assessments to better understand the causal relationships between vascularization, perfusion, and cognitive decline in CSVD. Integrating advanced imaging P. Arndt et al. NeuroImage 319 (2025) 121426

techniques such as functional MRI to assess cerebrovascular reactivity and neuronal network activity will provide a more comprehensive understanding of the underlying mechanisms. Additionally, using even higher resolution, such as 0.14 mm isotropic, and the application of motion correction would be advisable to segment vascularization even more precisely (Bollmann et al., 2022; Mattern et al., 2018). The exploration of potential therapeutic interventions with the aim to improve vascularization could offer new avenues for mitigating cognitive decline in patients with CSVD. Ultimately, a deeper understanding of the interplay between vascular health and cognitive function could lead to novel interventions that enhance brain resilience against CSVD and related pathologies.

Funding

The project has been supported by the Deutsche Alzheimer Gesell-schaft e.V. (DAlzG) and the Förderstiftung Dierichs (www.foerderstiftung-dierichs.de) (MD-DARS project) and by the German Research Foundation (DFG) (MA 9235/3-1/SCHR 1418/5-1 (501214112), CRC 1436 (B04, 425899996), and RTG 2413 (SynAGE, 362321501)).

Data availability

De-identified data are available from the corresponding author upon reasonable request.

CRediT authorship contribution statement

Philipp Arndt: Writing – review & editing, Writing – original draft, Visualization, Validation, Investigation, Formal analysis, Conceptualization. Stefanie Boewe: Methodology, Investigation, Formal analysis, Data curation. Jascha Brüggemann: Software, Methodology, Formal analysis, Data curation. Berta Garcia-Garcia: Writing - review & editing, Validation, Supervision, Software, Data curation, Conceptualization. Renat Yakupov: Writing – review & editing. Niklas Vockert: Writing - review & editing, Visualization. Anne Maas: Writing - review & editing. Malte Pfister: Writing – review & editing. Valentina Perosa: Writing - review & editing. Marwa Al Dubai: Writing - review & editing. Robin Jansen: Writing - review & editing. Sven G. Meuth: Writing - review & editing. Marc Dörner: Writing - review & editing. Patrick Müller: Writing - review & editing. Solveig Henneicke: Writing - review & editing. Frank Schreiber: Visualization, Software, Methodology, Data curation. Katja Neumann: Writing - review & editing, Visualization, Supervision, Software, Methodology, Formal analysis, Data curation. Hendrik Mattern: Writing - review & editing, Supervision, Software, Resources, Methodology, Data curation, Conceptualization. Stefanie Schreiber: Writing - review & editing, Resources, Project administration, Funding acquisition, Conceptualization.

Declaration of competing interest

The authors report no competing interests.

Acknowledgements

We are very grateful to all participants who volunteered to take part in the study.

Supplementary materials

Supplementary material associated with this article can be found, in the online version, at doi:10.1016/j.neuroimage.2025.121426.

References

- Afifi, A.K., 2003. The basal ganglia: a neural network with more than motor function. Semin. Pediatr Neurol. 10, 3–10. https://doi.org/10.1016/S1071-9091(02)00003-7
- Avants, B.B., Tustison, N.J., Song, G., Cook, P.A., Klein, A., Gee, J.C., 2011.
 A reproducible evaluation of ANTs similarity metric performance in brain image registration. Neuro. Image. 54, 2033–2044. https://doi.org/10.1016/j.neuroimage.2010.09.025.
- Bollmann, S., Mattern, H., Bernier, M., Robinson, S.D., Park, D., Speck, O., Polimeni, J.R., 2022. Imaging of the pial arterial vasculature of the human brain in vivo using highresolution 7T time-of-flight angiography. eLife 11. https://doi.org/10.7554/ eLife 71186
- Buxton, R.B., Frank, L.R., Wong, E.C., Siewert, B., Warach, S., Edelman, R.R., 1998. A general kinetic model for quantitative perfusion imaging with arterial spin labeling. Magn. Reson. Med. 40, 383–396. https://doi.org/10.1002/mrm.1910400308.
- Chappell, M.A., Groves, A.R., MacIntosh, B.J., Donahue, M.J., Jezzard, P., Woolrich, M. W., 2011. Partial volume correction of multiple inversion time arterial spin labeling MRI data. Magn. Reson. Med. 65, 1173–1183. https://doi.org/10.1002/mrm.22641.
- Chappell, M.A., Groves, A.R., Whitcher, B., Woolrich, M.W., 2009. Variational bayesian inference for a nonlinear forward model. IEEE Trans. Signal Process. 57, 223–236. https://doi.org/10.1109/TSP.2008.2005752.
- Chappell, M.A., MacIntosh, B.J., Donahue, M.J., Günther, M., Jezzard, P., Woolrich, M. W., 2010. Separation of macrovascular signal in multi-inversion time arterial spin labelling MRI. Magn. Reson. Med. 63, 1357–1365. https://doi.org/10.1002/mrm.22320.
- Chen, Y.-C., Wei, X.-E., Lu, J., Qiao, R.-H., Shen, X.-F., Li, Y.-H., 2019. Correlation between the number of lenticulostriate arteries and imaging of cerebral small vessel disease. Front. Neurol. 10, 882. https://doi.org/10.3389/fneur.2019.00882.
- Cho, Z.-H., Kang, C.-K., Han, J.-Y., Kim, S.-H., Kim, K.-N., Hong, S.-M., Park, C.-W., Kim, Y.-B., 2008. Observation of the lenticulostriate arteries in the human brain in vivo using 7.0T MR angiography. Stroke 39, 1604–1606. https://doi.org/10.1161/STROKEAHA.107.508002.
- Duering, M., Biessels, G.J., Brodtmann, A., Chen, C., Cordonnier, C., Leeuw, F.-E.de, Debette, S., Frayne, R., Jouvent, E., Rost, N.S., Telgte, A.ter, Al-Shahi Salman, R., Backes, W.H., Bae, H.-J., Brown, R., Chabriat, H., Luca, A.de, DeCarli, C., Dewenter, A., Doubal, F.N., Ewers, M., Field, T.S., Ganesh, A., Greenberg, S., Helmer, K.G., Hilal, S., Jochems, A.C.C., Jokinen, H., Kuijf, H., Lam, B.Y.K., Lebenberg, J., MacIntosh, B.J., Maillard, P., Mok, V.C.T., Pantoni, L., Rudilosso, S., Satizabal, C.L., Schirmer, M.D., Schmidt, R., Smith, C., Staals, J., Thrippleton, M.J., van Veluw, S.J., Vemuri, P., Wang, Y., Werring, D., Zedde, M., Akinyemi, R.O., Del Brutto, O.H., Markus, H.S., Zhu, Y.-C., Smith, E.E., Dichgans, M., Wardlaw, J.M., 2023. Neuroimaging standards for research into small vessel disease-advances since 2013. Lancet Neurol. 22, 602–618. https://doi.org/10.1016/S1474-4422(23)00131-Y
- El Falougy, H., Selmeciova, P., Kubikova, E., Haviarová, Z., 2013. The variable origin of the recurrent artery of Heubner: an anatomical and morphometric study. Biomed. Res. Int., 873434 https://doi.org/10.1155/2013/873434, 2013.
- Ell, S.W., Helie, S., Hutchinson, S., 2011. Contributions of the putamen to cognitive function. Horizon. Neurosci. Res. 7, 20, 2 bis.
- Engedal, T.S., Hjort, N., Hougaard, K.D., Simonsen, C.Z., Andersen, G., Mikkelsen, I.K., Boldsen, J.K., Eskildsen, S.F., Hansen, M.B., Angleys, H., Jespersen, S.N., Pedraza, S., Cho, T.H., Serena, J., Siemonsen, S., Thomalla, G., Nighoghossian, N., Fiehler, J., Mouridsen, K., Østergaard, L., 2018. Transit time homogenization in ischemic stoke - A novel biomarker of penumbral microvascular failure? J. Cerebral Blood Flow Metabolism. 38, 2006–2020. https://doi.org/10.1177/0271678X17721666.
- Fazekas, F., Chawluk, J.B., Alavi, A., Hurtig, H.I., Zimmerman, R.A., 1987. MR signal abnormalities at 1.5 T in Alzheimer's dementia and normal aging. AJR. Am. J. Roentgenol. 149, 351–356. https://doi.org/10.2214/ajr.149.2.351.
- Feekes, J.A., Hsu, S.-W., Chaloupka, J.C., Cassell, M.D., 2005. Tertiary microvascular territories define lacunar infarcts in the basal ganglia. Ann. Neurol. 58, 18–30. https://doi.org/10.1002/ana.20505.
- Feng, M., Wen, H., Xin, H., Zhang, N., Liang, C., Guo, L., 2021. Altered spontaneous brain activity related to neurologic dysfunction in patients with cerebral small vessel disease. Front. Aging Neurosci. 13, 731585. https://doi.org/10.3389/ fnagi.2021.731585.
- Fernando, J., Brown, R.B., Edwards, H., Egle, M., Markus, H.S., Tay, J., 2021. Individual markers of cerebral small vessel disease and domain-specific quality of life deficits. Brain Behav. 11, e02106. https://doi.org/10.1002/brb3.2106.
- Fischl, B., Salat, D.H., van der Kouwe, A.J.W., Makris, N., Ségonne, F., Quinn, B.T., Dale, A.M., 2004. Sequence-independent segmentation of magnetic resonance images. Neuro Image. 23 (Suppl 1), 69–84. https://doi.org/10.1016/j.neuroimage.2004.07.016.
- Folstein, M.F., Folstein, S.E., McHugh, P.R., 1975. "Mini-mental state". A practical method for grading the cognitive state of patients for the clinician. J. Psychiatr. Res. 12, 189–198. https://doi.org/10.1016/0022-3956(75)90026-6.
- Garcia-Garcia, B., Mattern, H., Vockert, N., Yakupov, R., Schreiber, F., Spallazzi, M., Perosa, V., Haghikia, A., Speck, O., Düzel, E., Maass, A., Schreiber, S., 2023. Vessel distance mapping: a novel methodology for assessing vascular-induced cognitive resilience. NeuroImage 274, 120094. https://doi.org/10.1016/j. neuroImage.2023.120094.
- Graybiel, A.M., 2000. The basal ganglia. Curr. Biology. 10, R509–R511. https://doi.org/10.1016/s0960-9822(00)00593-5.
- Groves, A.R., Chappell, M.A., Woolrich, M.W., 2009. Combined spatial and non-spatial prior for inference on MRI time-series. NeuroImage 45, 795–809. https://doi.org/ 10.1016/j.neuroimage.2008.12.027.

- Haast, R.A.M., Kashyap, S., Ivanov, D., Yousif, M.D., DeKraker, J., Poser, B.A., Khan, A. R., 2024. Insights into hippocampal perfusion using high-resolution, multi-modal 7T MRI. Proc. Natl. Acad. Sci. U.S.A. 121, e2310044121. https://doi.org/10.1073/pnas.2310044121.
- Huijts, M., Duits, A., Staals, J., Kroon, A.A., Leeuw, P.W.de, van Oostenbrugge, R.J., 2014. Basal ganglia enlarged perivascular spaces are linked to cognitive function in patients with cerebral small vessel disease. Curr. Neurovasc. Res. 11, 136–141. https://doi.org/10.2174/1567202611666140310102248.
- Jenkinson, M., Bannister, P., Brady, M., Smith, S., 2002. Improved optimization for the robust and accurate linear registration and motion correction of brain images. NeuroImage 17, 825–841. https://doi.org/10.1016/s1053-8119(02)91132-8.
- Jiang, S., Cao, T., Yan, Y., Yang, T., Yuan, Y., Deng, Q., Wu, T., Sun, J., Wu, S., Hao, Z.-L., Anderson, C.S., Wu, B., 2021. Lenticulostriate artery combined with neuroimaging markers of cerebral small vessel disease differentiate the pathogenesis of recent subcortical infarction. J. Cerebral Blood Flow Metabolism. 41, 2105–2115. https:// doi.org/10.1177/0271678X21992622.
- Jiang, S., Yan, Y., Yang, T., Zhu, Q., Wang, C., Bai, X., Hao, Z., Zhang, S., Yang, Q., Fan, Z., Sun, J., Wu, B., 2020. Plaque distribution correlates with morphology of lenticulostriate arteries in single subcortical infarctions. Stroke 51, 2801–2809. https://doi.org/10.1161/STROKEAHA.120.030215.
- Li, J., Bian, Y., Wu, F., Fan, Z., Zhang, C., Zhao, X., Ji, X., Yang, Q., 2024. Association of morphology of lenticulostriate arteries and proximal plaque characteristics with single subcortical infarction: a whole-brain high-resolution vessel wall imaging study. J. Am. Heart Assoc. 13, e032856. https://doi.org/10.1161/ JAHA 123.032856
- Li, Q., Yang, Y., Reis, C., Tao, T., Li, W., Li, X., Zhang, J.H., 2018. Cerebral small vessel disease. Cell Transplant. 27, 1711–1722. https://doi.org/10.1177/ 0063880718705148
- Li, X., Shen, M., Jin, Y., Jia, S., Zhou, Z., Han, Z., Zhang, X., Tong, X., Jiao, J., 2021. The effect of cerebral small vessel disease on the subtypes of mild cognitive impairment. Front Psychiat. 12, 685965. https://doi.org/10.3389/fpsyt.2021.685965.
- Ling, C., Fang, X., Kong, Q., Sun, Y., Wang, B., Zhuo, Y., An, J., Zhang, W., Wang, Z., Zhang, Z., Yuan, Y., 2019. Lenticulostriate arteries and basal ganglia changes in cerebral autosomal dominant arteriopathy with subcortical infarcts and leukoencephalopathy, a high-field MRI study. Front. Neurol. 10. https://doi.org/10.3389/fneur.2019.00870.
- Litak, J., Mazurek, M., Kulesza, B., Szmygin, P., Litak, J., Kamieniak, P., Grochowski, C., 2020. Cerebral small vessel disease. Int. J. Mol. Sci. 21. https://doi.org/10.3390/ ijms21249729.
- Marinkovic, S., Gibo, H., Milisavljevic, M., Cetkovic, M., 2001. Anatomic and clinical correlations of the lenticulostriate arteries. Clin. Anat. 14, 190–195. https://doi.org/ 10.1002/ca.1032.
- Mattern, H., Sciarra, A., Godenschweger, F., Stucht, D., Lüsebrink, F., Rose, G., Speck, O., 2018. Prospective motion correction enables highest resolution time-of-flight angiography at 7T. Magn. Reson. Med. 80, 248–258. https://doi.org/10.1002/ mrm 27033
- Max, J.E., Fox, P.T., Lancaster, J.L., Kochunov, P., Mathews, K., Manes, F.F., Robertson, B.A.M., Arndt, S., Robin, D.A., Lansing, A.E., 2002. Putamen lesions and the development of attention-deficit/hyperactivity symptomatology. J. Am. Acad. Child Adolesc. Psychiatry. 41, 563–571. https://doi.org/10.1097/00004583-200205000-00014.
- Ghandili, Mehrnoosh, Munakomi, Sunil, 2022. Neuroanatomy, putamen. In: Ghandili, M., Munakomi, S. (Eds.), StatPearls [Internet]. StatPearls Publishing.
- Meng, L., Zhao, J., Liu, J., Li, S., 2019. Cerebral small vessel disease and cognitive impairment. J. Neurorestoratol. 7, 184–195. https://doi.org/10.26599/ JNR 2019 9040023
- Morris, J.C., 1993. The Clinical Dementia Rating (CDR): current version and scoring rules. Neurology 43, 2412–2414. https://doi.org/10.1212/wnl.43.11.2412-a.
- Nasreddine, Z.S., Phillips, N.A., Bédirian, V., Charbonneau, S., Whitehead, V., Collin, I., Cummings, J.L., Chertkow, H., 2005. The Montreal Cognitive Assessment, MoCA: a brief screening tool for mild cognitive impairment. J. Am. Geriatr. Soc. 53, 695–699. https://doi.org/10.1111/j.1532-5415.2005.53221.x.
- Neumann, K., Schidlowski, M., Günther, M., Stöcker, T., Düzel, E., 2021. Reliability and reproducibility of Hadamard encoded pseudo-continuous arterial spin labeling in healthy elderly. Front Neurosci. 15, 711898. https://doi.org/10.3389/ fnins.2021.711898.

- Østergaard, L., Engedal, T.S., Moreton, F., Hansen, M.B., Wardlaw, J.M., Dalkara, T., Markus, H.S., Muir, K.W., 2016. Cerebral small vessel disease: capillary pathways to stroke and cognitive decline. J. Cerebral Blood Flow Metabolism. 36, 302–325. https://doi.org/10.1177/0271678X15606723.
- Pasi, M., Sugita, L., Xiong, L., Charidimou, A., Boulouis, G., Pongpitakmetha, T., Singh, S., Kourkoulis, C., Schwab, K., Greenberg, S.M., Anderson, C.D., Gurol, M.E., Rosand, J., Viswanathan, A., Biffi, A., 2021. Association of cerebral small vessel disease and cognitive decline after intracerebral hemorrhage. Neurology 96, e182–e192. https://doi.org/10.1212/WNL.0000000000011050.
- Patel, B., Markus, H.S., 2011. Magnetic resonance imaging in cerebral small vessel disease and its use as a surrogate disease marker. Int. J. Stroke. 6, 47–59. https://doi. org/10.1111/j.1747-4949.2010.00552.x.
- Perosa, V., Priester, A., Ziegler, G., Cardenas-Blanco, A., Dobisch, L., Spallazzi, M., Assmann, A., Maass, A., Speck, O., Oltmer, J., Heinze, H.-J., Schreiber, S., Düzel, E., 2020. Hippocampal vascular reserve associated with cognitive performance and hippocampal volume. Brain: A J. Neurol. 143, 622–634. https://doi.org/10.1093/ brain/awr383
- Potter, G.M., Chappell, F.M., Morris, Z., Wardlaw, J.M., 2015. Cerebral perivascular spaces visible on magnetic resonance imaging: development of a qualitative rating scale and its observer reliability. Cerebrovasc. Dis. 39, 224–231. https://doi.org/ 10.1150/000275153
- Prins, N.D., van Dijk, E.J., Heijer, T.den, Vermeer, S.E., Jolles, J., Koudstaal, P.J., Hofman, A., Breteler, M.M.B., 2005. Cerebral small-vessel disease and decline in information processing speed, executive function and memory. Brain: A J. Neurol. 128, 2034–2041. https://doi.org/10.1093/brain/awh553.
- Rosen, W.G., Mohs, R.C., Davis, K.L., 1984. A new rating scale for Alzheimer's disease. Am. J. Psychiat. 141, 1356–1364. https://doi.org/10.1176/ajp.141.11.1356.
- Schultz, W., 2016. Reward functions of the basal ganglia. J. Neural Transmis. (Vienna, Austria: 1996) 123, 679–693. https://doi.org/10.1007/s00702-016-1510-0.
- Seo, S.W., Kang, C.-K., Kim, S.H., Yoon, D.S., Liao, W., Wörz, S., Rohr, K., Kim, Y.-B., Na, D.L., Cho, Z.-H., 2012. Measurements of lenticulostriate arteries using 7T MRI: new imaging markers for subcortical vascular dementia. J. Neurol. Sci. 322, 200–205. https://doi.org/10.1016/j.ins.2012.05.032.
- Takata, K., Kimura, H., Ishida, S., Isozaki, M., Higashino, Y., Kikuta, K.-I., Okazawa, H., Tsujikawa, T., 2023. Assessment of arterial transit time and cerebrovascular reactivity in Moyamoya Disease by simultaneous PET/MRI. Diagnostics (Basel) 13. https://doi.org/10.3390/diagnostics13040756.
- Telgte, A.ter, van Leijsen, E.M.C., Wiegertjes, K., Klijn, C.J.M., Tuladhar, A.M., Leeuw, F.-E.de, 2018. Cerebral small vessel disease: from a focal to a global perspective. Nat. Rev. Neurol. 14, 387–398. https://doi.org/10.1038/s41582-018-0014-y.
- Tortorella, C., Romano, R., Direnzo, V., Taurisano, P., Zoccolella, S., Iaffaldano, P., Fazio, L., Viterbo, R., Popolizio, T., Blasi, G., Bertolino, A., Trojano, M., 2013. Load-dependent dysfunction of the putamen during attentional processing in patients with clinically isolated syndrome suggestive of multiple sclerosis. Mult. Scler. 19, 1153–1160. https://doi.org/10.1177/1352458512473671.
- Turner, R.S., Desmurget, M., 2010. Basal ganglia contributions to motor control: a vigorous tutor. Curr. Opin. Neurobiol. 20, 704–716. https://doi.org/10.1016/j. conb.2010.08.022.
- Viñas-Guasch, N., Wu, Y.J., 2017. The role of the putamen in language: a meta-analytic connectivity modeling study. Brain Struct. Funct. 222, 3991–4004. https://doi.org/ 10.1007/s00429-017-1450-y.
- Vockert, N., Perosa, V., Ziegler, G., Schreiber, F., Priester, A., Spallazzi, M., Garcia-Garcia, B., Aruci, M., Mattern, H., Haghikia, A., Düzel, E., Schreiber, S., Maass, A., 2021. Hippocampal vascularization patterns exert local and distant effects on brain structure but not vascular pathology in old age. Brain Communicat. 3, fcab127. https://doi.org/10.1093/braincomms/fcab127.
- Wei, N., Jing, J., Zhuo, Y., Zhang, Z., 2022. Morphological characteristics of lenticulostriate arteries in a large age-span population: results from 7T TOF-MRA. Front. Neurol. 13, 944863. https://doi.org/10.3389/fneur.2022.944863.
- Zhang, X., Liang, C., Wang, N., Wang, Y., Gao, Y., Sui, C., Xin, H., Feng, M., Guo, L., Wen, H., 2023. Abnormal whole-brain voxelwise structure-function coupling and its association with cognitive dysfunction in patients with different cerebral small vessel disease burdens. Front. Aging Neurosci. 15, 1148738. https://doi.org/10.3389/fnagi.2023.1148738.